Buildup and synchronization regimes of a vector pure-quartic soliton molecule in a fiber laser cavity

He, Chaojian; Zhu, Zhiwei; Yang, Song; Wang, Nan; Yang, Yingying; Lin, Xuechun

Published in:
Optics Express

Link to article, DOI:
10.1364/OE.520916

Publication date:
2024

Document Version
Publisher's PDF, also known as Version of record

Research Article | Vol. 32, No. 7 / 25 Mar 2024 / Optics Express 11895
Optics EXPRESS

Buildup and synchronization regimes of a vector pure-quartic soliton molecule in a fiber laser cavity

CHAOJIAN HE,[1,2,3,†] ZHIWEI ZHU,[4,†] SONG YANG,[5,6] NAN WANG,[1,2,3] YINGYING YANG,[1,2,3] AND XUECHUN LIN[1,2,3,7]

[1]*Laboratory of All-Solid-State Light Sources, Institute of Semiconductors, Chinese Academy of Sciences, Beijing 100083, China*
[2]*College of Materials Science and Opto-Electronic Technology, University of Chinese Academy of Sciences, Beijing 101407, China*
[3]*Beijing Engineering Technology Research Center of All-Solid-State Lasers Advanced Manufacturing, Beijing 100083, China*
[4]*Department of Mechanical and Automation Engineering, The Chinese University of Hong Kong, Hong Kong SAR, China*
[5]*DTU Electro, Department of Electrical and Photonics Engineering, Technical University of Denmark, DK-2800 Kgs. Lyngby, Denmark*
[6]*sonya@dtu.dk*
[7]*xclin@semi.ac.cn*
[†]The authors contributed equally to this work and are co-first authors.

Abstract: Pure-quartic solitons (PQSs) have recently received increasing attention due to their energy-width scaling over the traditional soliton, which has expanded our understanding of soliton dynamics with high-order dispersion in nonlinear systems. Here, we numerically reveal the asynchronization and synchronization processes of the sub-pulse within the vector PQS molecule in a mode-locked fiber laser by solving the coupled Ginzburg-Landau equations. During the establishment of a vector PQS molecule, the repulsion, attraction, and finally stabilization processes have been observed. Specifically, sub-pulse disappearance, regeneration, and finally synchronization with the other pulses are also investigated. Our analysis of the pulse energy, time interval, and relative phase evolution dynamics with the round trip indicates that the asynchronization and synchronization within the vector PQS molecule associate tightly with the gain competition and the cross-phase modulation. Our findings provide insights into the internal mutual dynamics within the vector soliton molecule and offer guidance for the applications of PQS.

1. Introduction

Optical solitons have been extensively studied in passive mode-locked fiber lasers due to their significant role in various fields, including ultrafast optics [1], nonlinear imaging [2,3], and optical frequency combs [4]. The dominant factors influencing the generation of traditional optical solitons in fiber lasers are negative second-order dispersion (β_2) and self-phase modulation (SPM) effect [5]. Through dispersion engineering, different types of optical solitons such as conventional solitons [6], similaritons [7], and dissipative solitons [8] were unveiled in fiber lasers. Compared to traditional solitons, pure-quartic solitons (PQSs) offer advantages such as higher pulse energy and a flatter spectral envelope [9,10]. These characteristics make PQS fiber lasers capable of generating high-peak-power pulses with a broader spectrum, which is suitable for applications in spectroscopy and optical communication [11,12]. The first experimental demonstration of a PQS fiber laser has been achieved by harnessing the interplay between fourth-order dispersion

#520916 https://doi.org/10.1364/OE.520916
Journal © 2024 Received 6 Feb 2024; revised 3 Mar 2024; accepted 3 Mar 2024; published 15 Mar 2024

Optics EXPRESS

(FOD) and nonlinearity, which is induced by pulse propagation inside a fiber laser cavity with the spectral pulse shaping [10].

Except for direct experimental investigation, numerical simulations and theoretical calculations [13–15] have also been regarded as effective tools for analyzing soliton dynamics, especially when exploring the detailed effects of specific parameters in complex nonlinear systems, such as the generation of dissipative PQS [16], pulsating dynamics [17], creeping and erupting dynamics [18], and dissipative PQS resonance [19].

Previous studies primarily focused on investigating the properties of scalar PQS propagation along a single optical fiber. The properties of the propagation of the scalar PQS in passive quartic dispersion fibers [9], self-similar propagation of optical pulses in positive quartic-dispersion active fibers [20] have been investigated. Meanwhile, the weak birefringent effect within a fiber laser cavity significantly influences soliton generation and propagation dynamics. Generally, the single-mode fiber generally supports two orthogonal polarization modes owing to its birefringence, in which the cross-phase modulation (XPM) should be considered. *C. X. Yang et al.* have theoretically investigated the vector properties of quartic solitons in a pure fourth-order-dispersion birefringent fiber [21], and revealed the collision dynamics of vector solitons in dissipative systems [22]. However, they only studied vector quartic solitons but not soliton molecules and their generation dynamics. Earlier in our work, we demonstrated the observation of stationary and pulsating vector PQS molecules in a weakly-birefringent fiber cavity [23], which shows the effect of different gains on the output of the pulse. However, the detailed generation and evolution dynamics of the PQS molecule, presenting a fascinating opportunity to expand our understanding of the general dynamics of complex nonlinear systems, have not been fully investigated.

In this letter, we investigate the asynchronization and synchronization processes of the sub-pulses within a vector PQS molecule. In the initial stage of oscillation, the sub-pulses experience an asynchronous state, in which the temporal separation and the relative phase change with the increase of the roundtrip numbers; as oscillating, the temporal separation and the relative phase gradually turn into stable; finally, the temporal separation and relative phase in both axes are fixed, and a stable PQS is obtained. Additionally, the disappearance and reappearance operations of the sub-pulse within the vector PQS molecule are observed and investigated. We have discovered that the evolution and dynamics of vector PQSs are related to the energy exchange induced by XPM. The energy redistribution of the sub-pulses with increasing the roundtrip number provides new perspectives on the physical mechanism of the vector PQS generation.

2. Numerical methods

Our model is based on the classical all-fiber erbium-doped mode-locked laser structure, as shown in Fig. 1, which is similar to that used in previous PQS laser system [23]. The system consists of 1-m erbium-doped fiber (EDF), a saturable absorber (SA), 3-m of single-mode fiber (SMF), and an output coupler (OC), which is set to be 20%. Here, we simplified the commonly used unidirectional isolator, but still only considered the propagation along clockwise direction in the cavity. The fiber birefringence effect is fully taken into account, and the soliton dynamics inside the laser cavity are determined by the coupled Ginzburg-Landau equations [24,25]:

$$\frac{\partial A_x}{\partial z} = \frac{1}{2}\Delta\beta_1\frac{\partial A_x}{\partial T} - \frac{i\beta_2}{2}\frac{\partial^2 A_x}{\partial T^2} + \frac{\beta_3}{6}\frac{\partial^3 A_x}{\partial T^3} + \frac{i\beta_4}{24}\frac{\partial^4 A_x}{\partial T^4} + \frac{g-\alpha}{2}A_x + \frac{g}{2\Omega_g^2}\frac{\partial^2 A_x}{\partial T^2} + i\gamma\left(|A_x|^2 + \frac{2}{3}|A_y|^2\right)A_x + \frac{i\gamma}{3}A_x^* A_y^2 \exp(-2i\Delta\beta z)$$

Optics EXPRESS

$$\frac{\partial A_y}{\partial z} = -\frac{1}{2}\Delta\beta_1\frac{\partial A_y}{\partial T} - \frac{i\beta_2}{2}\frac{\partial^2 A_y}{\partial T^2} + \frac{\beta_3}{6}\frac{\partial^3 A_y}{\partial T^3} + \frac{i\beta_4}{24}\frac{\partial^4 A_y}{\partial T^4} + \frac{g-\alpha}{2}A_y + \frac{g}{2\Omega_g^2}\frac{\partial^2 A_y}{\partial T^2}$$
$$+ i\gamma\left(|A_y|^2 + \frac{2}{3}|A_x|^2\right)A_y + \frac{i\gamma}{3}A_y^* A_x^2 \exp(2i\Delta\beta z)$$

where A_x and A_y are the slowly varying amplitudes of the two pulse envelopes along the slow and fast axes of birefringent fibers; β_2, β_3, and β_4 denote the second-, third-, and fourth-order dispersion of the fiber respectively. Considering the advanced optical fiber technique, β_2 and β_3 are set as 0 in our calculation [16,26]. α, and γ are the loss, nonlinear coefficient of the fiber respectively; Ω_g is the gain bandwidth of the gain fiber and g is the saturable gain for the EDF, which can be expressed as [27]:

$$g = g_0 \exp\left(-\frac{\int (|A_x|^2 + |A_y|^2)dt}{E_{sat}}\right)$$

where g_0 is the small signal gain; E_{sat} is the saturable energy of the EDF and related to the pump strength; $\Delta\beta$ and $\Delta\beta_1$ are related to the linear birefringence and given by [28,29]:

$$\Delta\beta = \beta_{0x} - \beta_{0y} = \frac{\omega_0}{c}B_m$$
$$\Delta\beta_1 = \beta_{1x} - \beta_{1y} = \frac{B_m}{c}$$

where c is the light speed; ω_0 is the central optical frequency; B_m is the strength of modal birefringence, which is defined as:

$$B_m = n_x - n_y$$

where n_x and n_y are the modal refractive indices along the slow axis x and the fast axis y. The SA is the mode-locker and has a transmission function for the pulse amplitude:

$$T = 1 - \frac{q_0}{1 + (|A_x|^2 + |A_y|^2)/P_{sat}}$$

where q_0 and P_{sat} represent modulation depth and saturation power of the SA, respectively [30,31]. In our simulation, q_0 = 0.53 and P_{sat} = 120 W. The simulations are performed using MATLAB v2020a.

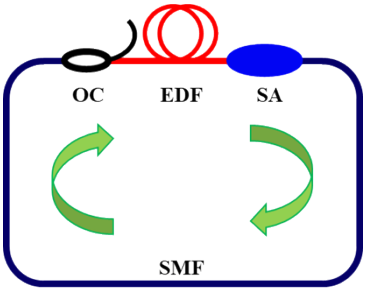

Fig. 1. Schematic of the passively mode-locked fiber laser for simulations. $\beta_{2-EDF} = \beta_{2-SMF} = 0$ ps^2/km; $\beta_{3-EDF} = \beta_{3-SMF} = 0$ ps^3/km; $\beta_{4-EDF} = \beta_{4-SMF} = -10$ ps^4/km; $\gamma_{-EDF} = \gamma_{-SMF} = 3$ W/km; $\alpha = 0$ dB/km; $\Omega_g = 49$ nm; $w_0 = 1207.69$ THz; $g_0 = 3000$ /km; $c = 3 \times 10^5$ km/s; $B_m = 5 \times 10^{-8}$; $E_{sat} = 271$ pJ.

Optics EXPRESS

3. Results and discussions

As far as we know, the energy of traditional solitons is constrained by the soliton area theorem when they exist in stable evolution within nonlinear systems. With the energy over a certain threshold, the soliton will split, leading to the formation of a multiple-soliton state [32]. The simulation starts with an initial weak pulse: $A = \mathrm{sqrt}(P_0) \times \mathrm{sech}(t/t_s)$, where P_0 is 0.0001 W and t_s is 2 ps. Meanwhile, the time window size of the simulation is 64 ps. For different optical parameters, vector soliton molecules have similar dynamic characteristics [23]. However, there is no detailed analysis of the detailed evolution process of sub-pulses. In order to facilitate research, according to our simulations, the E_{sat} is set as 271 pJ to promote the soliton splitting for the generation of the vector PQS molecule. The length of spatial step is 1 mm. Figure 2 presents the entire buildup process of the vector PQS molecule in the mode-locked fiber laser. The polarization-resolved pulses along the two axes show the evolution processes that are interrelated but have distinct characteristics, as demonstrated in Figs. 2(a) and 2(b). Obvious asynchronization and synchronization [33,34] process can be observed, which mainly involves soliton splitting, repulsion, attraction, and the eventual generation of a stable vector PQS molecule.

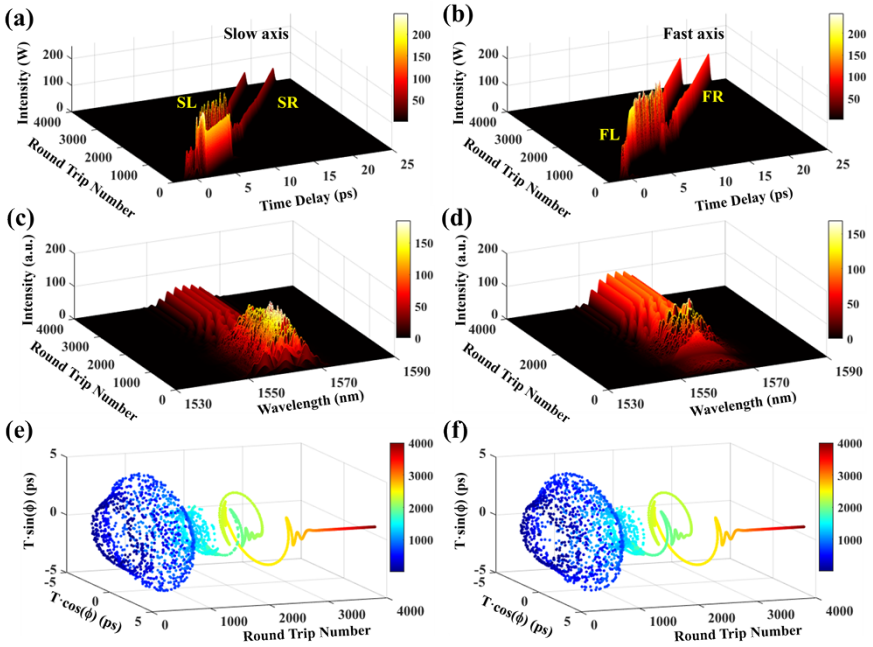

Fig. 2. The entire buildup process of vector PQS molecules in a mode-locked laser. The temporal evolution of sub-pulses on the (a) slow and (b) fast axes; The spectral evolution of sub-pulses on the (c) slow and (d) fast axes; 3D scatter diagram of the soliton interaction on the (e) slow and (f) fast axes.

Specifically, under a strengthened pump setting, the initial single pulse rapidly splits into two pulses within approximately 20 round trips for two axes. The intensity of the four PQSs undergoes continuous evolution, reshaping until stabilization around 2900$^{\mathrm{th}}$ round trip. After the 2900$^{\mathrm{th}}$ round trip, the shapes of the sub-pulses, the temporal separation and the relative phase on both axes tend to be stabilized, indicating the complete synchronization of the sub-pulse in the molecule and the obtainment of a stable vector PQS molecule. During the buildup process, the two sub pulses initially repel each other between the 20$^{\mathrm{th}}$ and 650$^{\mathrm{th}}$ round trips; after that, the two sub pluses within the molecule start to attract each other, which can also be concluded in

Optics EXPRESS

Figs. 2(e) and 2(f), where T is the separation between two solitons and Φ is the relative phase. The emission spectra of the vector PQS molecules on the slow and fast axes are depicted in Figs. 2(c) and 2(d), respectively. These spectra exhibit characteristics of a transient bound state prior to the establishment of a stationary vector PQS molecule.

However, an intriguing phenomenon within the vector PQS molecule generation process deserves attention. Between the 20^{th} and 1000^{th} round trips, the laser component on the slow axis exhibits a dual-pulse characteristic, while that on the fast axis features a single-pulse operation since the right pulse on the fast axis (FR) disappears. This can be attributed to failure of FR in the gain competition. However, according to the temporal position and delayed direction, the single PQS on the fast axis has the same evolutionary trajectory in the time domain with the left pulse on the slow axis (SL), indicating that these two pulses have been nearly trapped together due to the weak birefringence of the optical fiber. Interestingly, after the 1000^{th} round trip, the disappeared pulse reappears on the fast axis, almost synchronously with the right pulse on the slow axis (SR). The regeneration of FR is a result of achieving a balanced state between the two axes and is related to the energy exchange involved in the process of establishing stable vector soliton molecules. This intricate yet captivating process of the vector PQS molecule generation is intricately linked to the interaction among the four sub-pulses, which will be elaborated on in detail in the subsequent section.

To better analyze the formation of the vector PQS molecule, the evolution processes at different stages are sliced and magnified to reveal more details of the soliton dynamics. The slices of vector PQS molecule generation before the 650^{th} round trip is depicted in Fig. 3, which demonstrate that the sub-pulses in the vector PQS molecule are asynchronous. The two pulses on the slow axis have an increasing temporal separation distance with the increase in the round trip. The exclusionary trend and weak coherence within the molecule results in the failure to bound the two PQSs together. It is obvious that the laser energy on the slow axis is more predominantly distributed to the SR. The corresponding spectrum modulation on the slow axis has also been observed in Fig. 3(b). In contrast, the evolution dynamics of sub-pulses on the fast axis during the same period are completely different. The fast axis component is characterized by a single PQS operation since the right pulse is not obvious after the initial splitting and oscillating, indicating that the laser energy on the fast axis is almost entirely concentrated on the FL. The absence of noticeable interference patterns in the spectrum provides further confirmation of the near-single-pulse state for the fast axis. Another noteworthy phenomenon is that the SL and FL exhibit very similar temporal evolution paths, indicating that the XPM induced by the weak birefringence successfully promotes pulse trapping. The birefringence effect dominates the gain competition for pulse evolution and energy distribution during the period, whereas the interaction between sub-pulses inside the molecules is relatively weaker. The exclusion and weak coupling of sub-pulses inside the molecules can be further demonstrated in Figs. 3(c) and 3(f), which present the top views of the soliton interaction on slow and fast axes. Due to the near disappearance of the FR, we extract the pulse position and phase by utilizing the component on the fast axis of the right pulse in the vector PQS molecule. The diffusion trend observed in the soliton interaction further illustrates the asynchronous nature of the sub pulses. It can also be inferred that the temporal evolution is dominated by the slow axis during this period according to the similar interaction on two axes, which is attributed to the significant energy difference between the two axes.

Examining the evolution of pulse energy can provide an alternative perspective on the soliton dynamics involved in generating vector PQS molecules and deepen our understanding of underlying physics. Figure 4 presents the energy evolution of the four sub pulses over the whole 4000 round trips. The energy of SR remains relatively stable between the 20^{th} and 650^{th} round trips, while a distinct complementary operation is observed between SL and FL, characterized by a violent oscillation that tends to become gentle. This phenomenon indicates an energy exchange

Optics EXPRESS

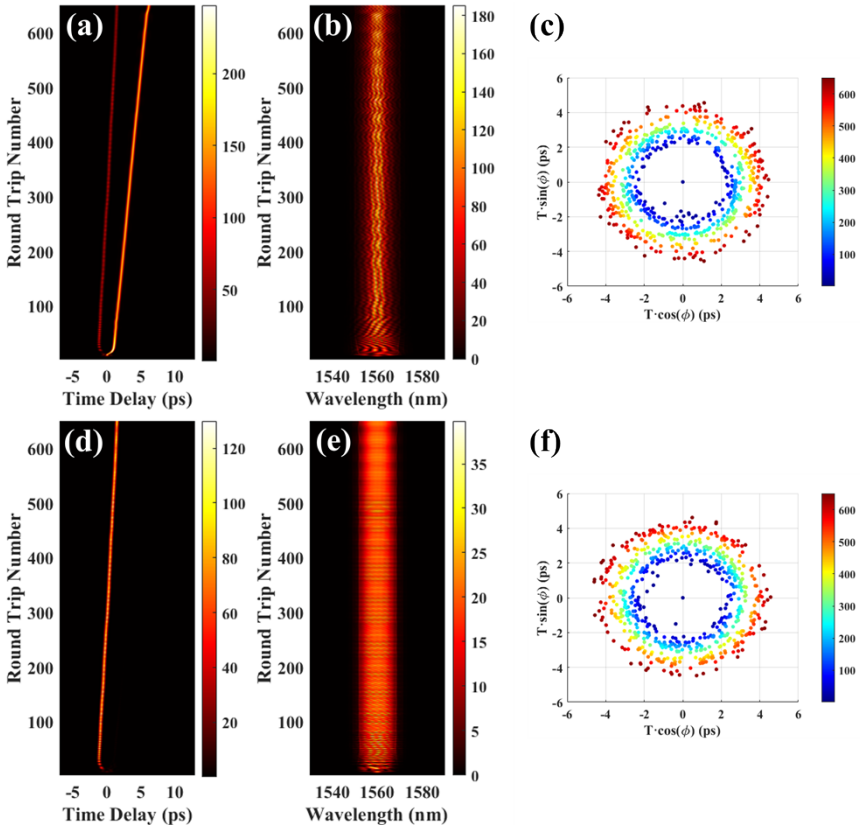

Fig. 3. Polarization-resolved vector PQS molecule evolution in the time and frequency domain, and corresponding top views of the soliton interaction the first 650 round trips on (a, b, c) slow and (d, e, f) fast axes.

that occurs due to XPM induced by the birefringence effect. In addition, the energy of FR is notably lower compared to the other three pulses, as it fails to gain competitive advantage within the vector pulse packet. The energy of SR, on the other hand, is significantly higher than that of the other sub-pulses on both the slow and fast axes, indicating its competitive advantage of SR within the vector PQS molecule. Between the 650th to 1000th round trips, a notable distinction of pulse evolution is that the consistent reduction in the temporal interval distance and obvious attraction between the sub-pulses as the roundtrip number increases, as depicted in Fig. 5, which mean that the sub-pulses on both axes slowly begin to synchronize. Within this stage, the intensity of the FR is still too weak to be observed in Fig. 5(d). The spectra evolutions on the two axes are shown in Figs. 5(b) and 5(e). On the slow axis, there is a distinct interference pattern resulting from the presence of the PQS molecule. The instability observed in the emission spectrum can be attributed to intense gain competition and energy redistribution among the four sub-pulses. However, the near-single-pulse state persists on the fast axis during the 650th to 1000th round trip, because of the relatively low energy of the FR. The instability observed in the spectrum on fast axis mainly arises from the enhanced energy transfer. For instance, the energy of the SR gradually decreases and then enters a period of intense oscillations, while that of the FL increases during this period. Despite the FR starting to regenerate during intense energy redistribution, the energy remains too low to be observed in the evolution trace.

Optics EXPRESS

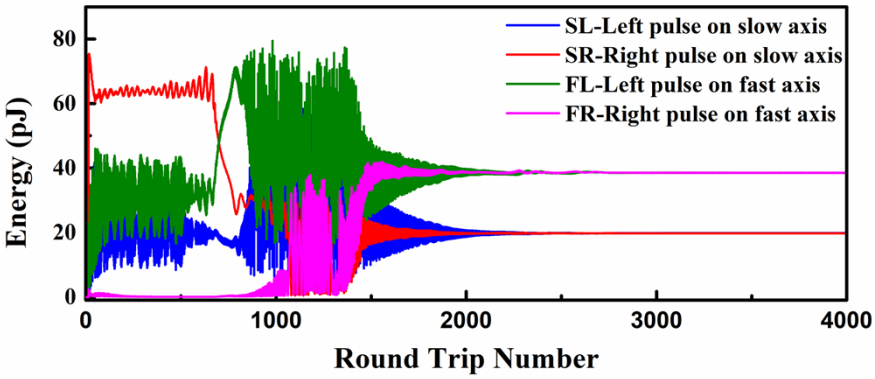

Fig. 4. The energy of the four pulses evolution with the increase of the round trip number when $E_{sat} = 271$ pJ.

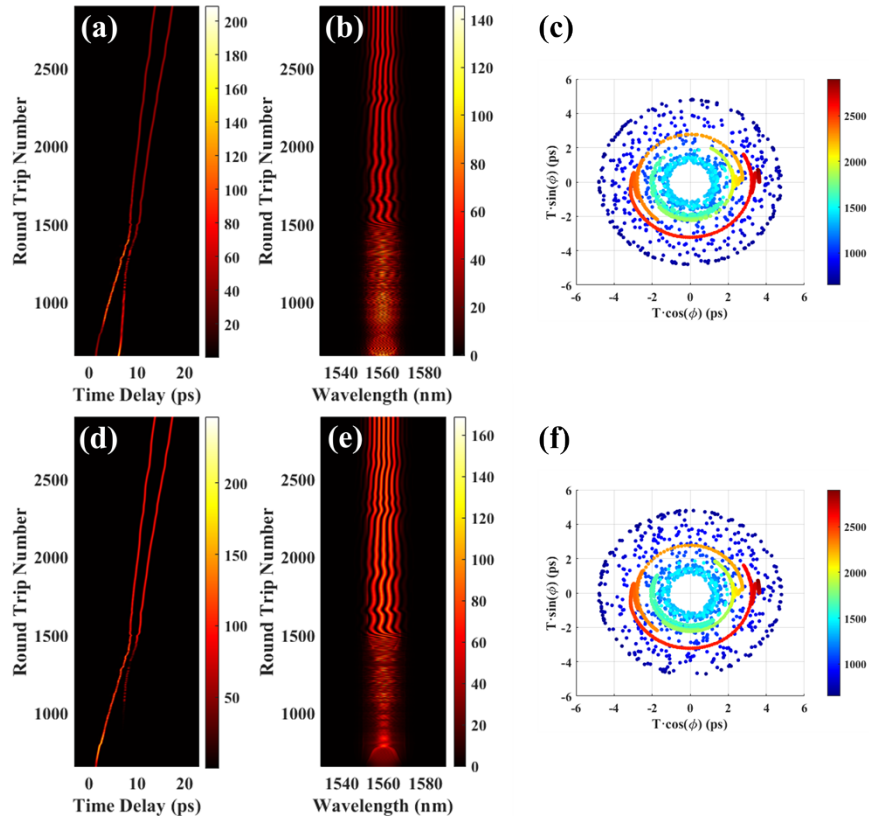

Fig. 5. Polarization-resolved vector PQS molecule evolution in the time and frequency domain, and corresponding top views of the soliton interaction from the 650th to 2900th round trip on (a, b, c) slow and (d, e, f) fast axes.

Optics EXPRESS

A significant shift in behavior occurs between the 1000th and 2900th round trip, as the gain competition mechanism becomes more intricate during this stage. The energy of the sub-pulses on both the fast and slow axes exhibits violent oscillations, as depicted in Fig. 4. Of particular note is the appearance of the FR, as illustrated in Fig. 5(d), which is an intriguing phenomenon. Transient bound states are clearly observed in two axes, indicating that the energy of the FR is sufficiently large to generate a distinct interference pattern. There are two reasons for the FR regeneration. The first is that due to the interaction among pulses, the energy of the other three pulses can be transferred to the FR through XPM within the vector molecule, resulting in an increase in its intensity. The second reason is related to the characteristics of the PQS itself. Owing to the long oscillating tail of the PQS, it's easier to induce new soliton from the noise background when suitable phase-matching is achieved for the XPM and degenerate four-wave mixing in birefringent fibers [10,35,36]. This is further substantiated by the fact that the regenerated FR has the same position as the SR in the time domain. The two reasons respectively focus on the soliton amplification and soliton regeneration, which can both contribute to the reappearance of solitons. After the four-pulse state is re-established, the temporal separation and relative phase gradually stabilize, and the four pulses start to turn into synchronization, as illustrated Figs. 5(c) and 5(f).

Around the 2900th round trip, the stationary vector PQS molecule is obtained, as evidenced by the stability of the temporal and spectral shapes, as depicted in Fig. 6. Furthermore, the temporal separation distance and relative phase of the two sub-pulses inside the two orthogonal PQS molecules, illustrated in Figs. 6(c) and 6(f), remain fixed simultaneously after the 2900th round trip. These evolution results demonstrate that the four pulses have been bound together with the determined phase relationship, while the soliton trapping inside the molecule and between the two axes in a weak-birefringence fiber has been realized for the generation of a stable vector PQS molecule. Additionally, the spectral and temporal output of the polarization-resolved vector PQS molecule at the 4000th round trip are presented in Figs. 6(g) and 6(h), providing further insight into its characteristics. Both pulses on both axes exhibit identical physical properties in the time domain, such as pulse duration and intensity, confirming the observations on the soliton energy quantization effect. The obvious temporal oscillating tails can be observed from Fig. 6(i), confirming the PQS generation. Overall, $E_{left-fast} \approx E_{right-fast} > E_{left-slow} \approx E_{right-slow}$, and the fast axis has gained more energy than the slow axis.

Observing and analyzing the synchronization and asynchronization processes during the establishment of the vector PQS molecule, including soliton splitting, repulsion, attraction, and the regeneration, enriches the more complex vectorial behaviors based on the existing dynamics research of soliton molecules [37,38]. Our results also theoretically demonstrate the novel soliton molecule based on the PQS, revealing the significant role of high-order dispersion in the formation process of vector soliton molecules. To further investigate the vector nature for deep insight into the synchronization and asynchronization processes of the PQS molecule, we trace the trajectories of the Stokes vector on the Poincaré sphere respectively for the left and right sub pulses, as shown in Fig. 7. Considering the variations in energy and positions of the pulses during the evolution process, we choose the normalized Stokes vector at the peaks of the sub pulses. Components of the Stokes vector with the magnitude S_0 are calculated according to the definitions:

$$S_0 = |A_x|^2 + |A_y|^2, \quad S_1 = |A_x|^2 - |A_y|^2$$
$$S_2 = 2\mathrm{Re}(A_x A_y^*), \quad S_3 = -2\mathrm{Im}(A_x A_y^*)$$

During the first 650th round trips, the state of polarization (SOP) of the left and right sub pulses exhibits characteristics of independent evolution in Figs. 7(a) and 7(b). Due to the closely matched energy distribution of the left pulse on both axes, the overall evolution trend of the SOP transitions from a chaotic random distribution to a concentrated polarization state, specifically on

Optics EXPRESS

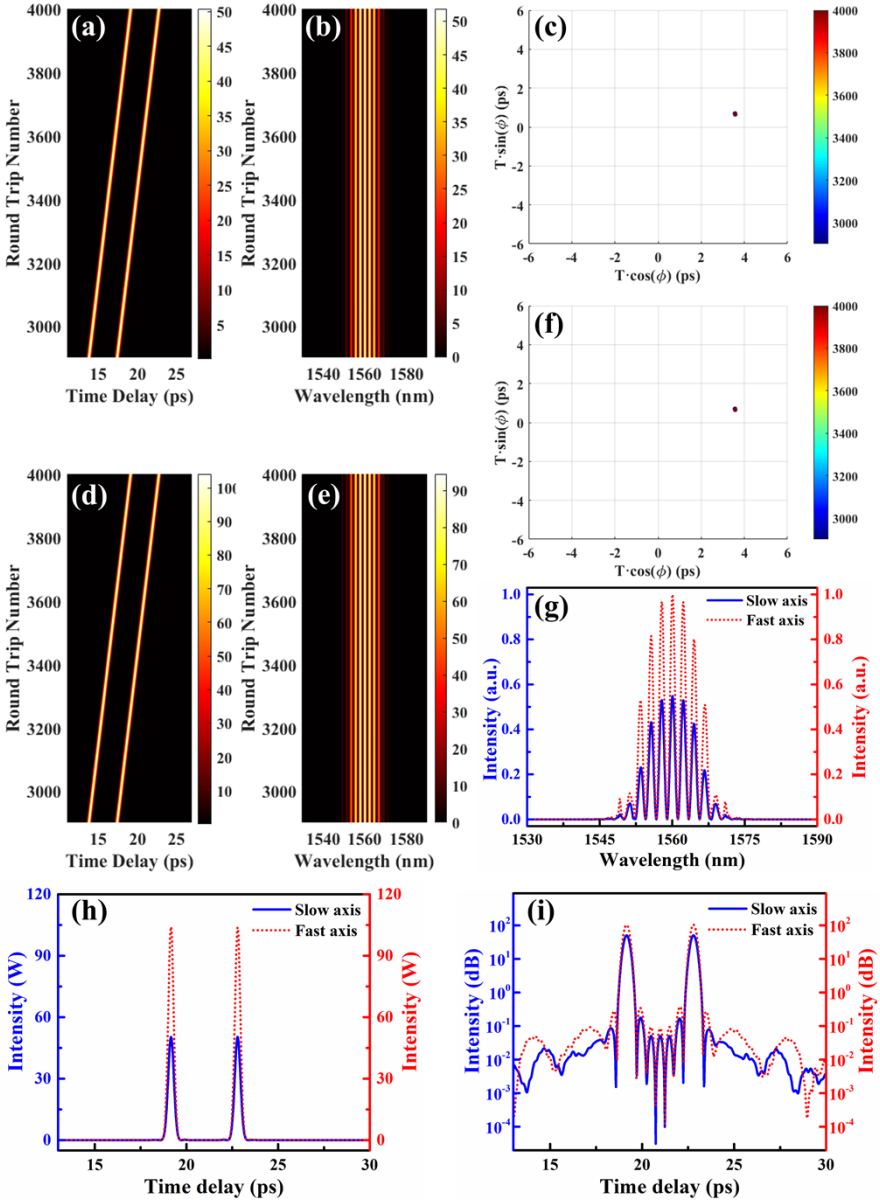

Fig. 6. Polarization-resolved vector PQS molecule evolution in the time and frequency domain, and corresponding top views of the soliton interaction from the 2900th to 4000th round trip on (a, b, c) slow and (d, e, f) fast axes. (g) The spectra of the polarization-resolved vector PQS molecule output from the 4000th round trip. (h, i) The pulse shapes of the polarization-resolved vector PQS molecule output from the 4000th round trip.

Optics EXPRESS

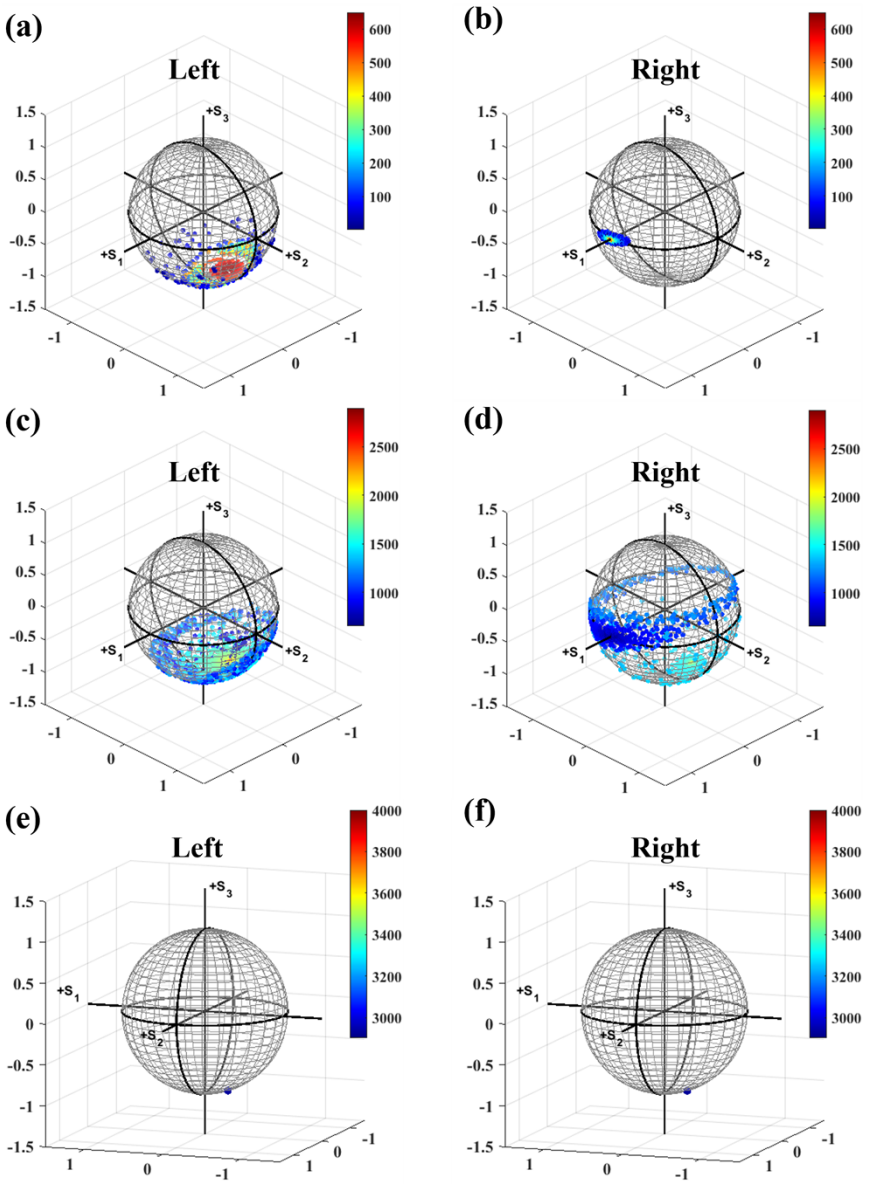

Fig. 7. The SOP evolution of the (a) left and (b) right sub pulses from the 0th to 650th round trip. The SOP evolution of the (c) left and (d) right sub pulses from the 650th to 2900th round trip. The SOP evolution of the (e) left and (f) right sub pulses from the 2900th to 4000th round trip.

Optics EXPRESS

the lower half surface of the Poincaré sphere. On the other hand, the energy of the right pulse is mainly concentrated on the slow axis, resulting in small fluctuations of the SOP around a single linear polarization state. When it comes to the second stage from the 650th to 2900th round trip in Figs. 7(c) and 7(d), the independence of the SOP evolution for two sub pulses is disrupted and the soliton synchronization is gradually established. During this period, the SOP of the left sub pulse breaks away from the previous stabilization trend, diffuses into a random distribution on the lower half surface again, and then gradually converges towards a fixed polarization state. Conversely, the right sub pulse starts from the previous linear polarization state and the SOP evolves along a circular trajectory on the upper half surface. However, during the process of synchronization establishment, the SOP is pulled back towards the lower half surface, aligning with the left sub pulse, and gradually approaching the same polarization state. It can be observed that due to the regeneration of the FR along with the influx of energy, the evolution of the SOP between the left and right sub pulses begins to exhibit correlation and eventually converges to a consistent state, which is more obvious in Figs. 7(e) and 7(f) for the stable vector PQS molecule. In subsequent simulations, we also explored the evolution results under the high pump power with E_{sat} from 240 pJ to 300 pJ. The formation of stable PQS molecules were observed between 266 pJ and 271 pJ with similar asynchronous and synchronous behaviors, while exhibited the non-stable pulsating states for other pump values [39]. It demonstrates that the formation of the new type of soliton molecule is not an exceptional case, but rather sensitive to the energy parameter.

4. Conclusions

In conclusion, we have demonstrated the asynchronization and synchronization processes during the buildup of the vector PQS molecule in the mode-locked fiber laser, which promotes a significant advancement in the field of soliton dynamics of PQSs in birefringent optical fibers. The dynamics mainly involved the sub-pulses generation, dynamic evolution, and the eventual formation into a stable vector PQS molecule. Additionally, we observed the disappearance and regeneration operations of the sub-pulse within the vector PQS molecule. This sub-pulse finally has a fixed temporal relationship with other pulses, which also features the evolution process from asynchronization to synchronization. We reveal that the generation of the stable vector PQS molecule is closely associated with the complex gain competition dynamics resulting from the XPM within the entire vector PQS molecule. These results provide deeper insights into the internal mutual dynamics within the vector soliton molecule, which, in turn, can serve as valuable guidance for the practical applications of PQSs.

Funding. National Natural Science Foundation of China (62175230, 62225507, U2033211); Innovation Fund Demark (2105-00039B: Hypersort); Villum Fonden (00037822: Table-Top Synchrotrons); CAS Project for Young Scientists in Basic Research (YSBR-065).

Disclosures. The authors declare no conflicts of interest.

Data availability. Data underlying the results presented in this paper are not publicly available at this time but may be obtained from the authors upon reasonable request.

References

1. P. Grelu and N. Akhmediev, "Dissipative solitons for mode-locked lasers," Nat. Photonics **6**(2), 84–92 (2012).
2. C. Xu and F. W. Wise, "Recent advances in fibre lasers for nonlinear microscopy," Nat. Photonics **7**(11), 875–882 (2013).
3. C. Kong, C. Pilger, H. Hachmeister, *et al.*, "High-contrast, fast chemical imaging by coherent Raman scattering using a self-synchronized two-colour fibre laser," Light: Sci. Appl. **9**(1), 25 (2020).
4. X. Yi, Q. F. Yang, K. Y. Yang, *et al.*, "Soliton frequency comb at microwave rates in a high-Q silica microresonator," Optica **2**(12), 1078–1085 (2015).
5. Y. Zhao, W. Wang, X. H. Li, *et al.*, "Functional Porous MOF-Derived CuO Octahedra for Harmonic Soliton Molecule Pulses Generation," ACS Photonics **7**(9), 2440–2447 (2020).
6. Y. Cui and X. Liu, "Graphene and nanotube mode-locked fiber laser emitting dissipative and conventional solitons," Opt. Express **21**(16), 18969–18974 (2013).

Optics EXPRESS

7. J. M. Dudley, C. Finot, D. J. Richardson, *et al.*, "Self-similarity in ultrafast nonlinear optics," Nat. Phys. **3**(9), 597–603 (2007).
8. M. Nie, B. Li, K. Jia, *et al.*, "Dissipative soliton generation and real-time dynamics in microresonator-filtered fiber lasers," Light: Sci. Appl. **11**(1), 296 (2022).
9. K. K. K. Tam, T. J. Alexander, A. Blanco-Redondo, *et al.*, "Stationary and dynamical properties of pure-quartic solitons," Opt. Lett. **44**(13), 3306–3309 (2019).
10. A. F. J. Runge, D. D. Hudson, K. K. K. Tam, *et al.*, "The pure-quartic soliton laser," Nat. Photonics **14**(8), 492–497 (2020).
11. K. W. Liu, S. Y. Yao, and C. X. Yang, "Raman pure quartic solitons in Kerr microresonators," Opt. Lett. **46**(5), 993–996 (2021).
12. S. Yang, Z. Zhu, C. He, *et al.*, "Collapse of pure-quartic solitons in a mode-locked fiber laser," Chaos, Solitons Fractals **180**, 114538 (2024).
13. K. K. K. Tam, T. J. Alexander, A. Blanco-Redondo, *et al.*, "Generalized dispersion Kerr solitons," Phys. Rev. A **101**(4), 043822 (2020).
14. B. A. Malomed, "Bound solitons in the nonlinear Schrödinger-Ginzburg-Landau equation," Phys. Rev. A **44**(10), 6954–6957 (1991).
15. B. A. Malomed, "Bound solitons in coupled nonlinear Schrödinger equations," Phys. Rev. A **45**(12), R8321–R8323 (1992).
16. Z. C. Qian, M. Liu, A. P. Luo, *et al.*, "Dissipative pure-quartic soliton fiber laser," Opt. Express **30**(12), 22066–22073 (2022).
17. Z. X. Zhang, M. Luo, J. X. Chen, *et al.*, "Pulsating dynamics in a pure-quartic soliton fiber laser," Opt. Lett. **47**(7), 1750–1753 (2022).
18. Y. Han, B. Gao, G. Wu, *et al.*, "Creeping and erupting dynamics in a pure-quartic soliton fiber laser," Opt. Express **31**(2), 1787–1798 (2023).
19. Y. S. Zhang, C. H. Jin, C. N. Tao, *et al.*, "Dissipative pure-quartic soliton resonance in an Er-doped fiber laser," Opt. Commun. **538**, 129479 (2023).
20. A. F. J. Runge, T. J. Alexander, J. Newton, *et al.*, "Self-similar propagation of optical pulses in fibers with positive quartic dispersion," Opt. Lett. **45**(13), 3365–3368 (2020).
21. K. J. Zhao, C. X. Gao, X. S. Xiao, *et al.*, "Vector quartic solitons in birefringent fibers," Opt. Lett. **46**(4), 761–764 (2021).
22. K. J. Zhao, C. X. Gao, X. S. Xiao, *et al.*, "Real-time collision dynamics of vector solitons in a fiber laser," Photonics Res. **9**(3), 289–298 (2021).
23. Z. Zhu, S. Yang, C. He, *et al.*, "Vector pure-quartic soliton molecule fiber laser," Chaos, Solitons Fractals **175**, 113978 (2023).
24. X. Hu, J. Guo, J. Wang, *et al.*, "Novel optical soliton molecules formed in a fiber laser with near-zero net cavity dispersion," Light: Sci. Appl. **12**(1), 38 (2023).
25. G. P. Agrawal, *Nonlinear Fiber Optics*, 5th ed. (Academic, 2013).
26. C. M. de Sterke, A. F. Runge, D. D. Hudson, *et al.*, "Pure-quartic solitons and their generalizations—Theory and experiments," APL Photonics **6**(9), 091101 (2021).
27. Y. F. Wang, L. Su, S. Wang, *et al.*, "Breach and recurrence of dissipative soliton resonance during period-doubling evolution in a fiber laser," Phys. Rev. A **102**(1), 013501 (2020).
28. Z. Zhu, S. Yang, C. He, *et al.*, "Cavity-birefringence-dependent vector pure-quartic soliton fiber laser," Opt. Express **31**(22), 35529–35541 (2023).
29. D. Mao, Z. He, Y. Zhang, *et al.*, "Phase-matching-induced near-chirp-free solitons in normal-dispersion fiber lasers," Light: Sci. Appl. **11**(1), 25 (2022).
30. C. Ma, X. Tian, B. Gao, *et al.*, "Dynamic evolution of the dissipative soliton in passively mode-locked fiber laser based on black phosphorus as a new saturable absorber," Opt. Commun. **406**, 177–182 (2017).
31. Q. Bao, H. Zhang, J. X. Yang, *et al.*, "Graphene–Polymer Nanofiber Membrane for Ultrafast Photonics," Adv. Funct. Mater. **20**(5), 782–791 (2010).
32. W. H. Renninger, A. Chong, and F. W. Wise, "Area theorem and energy quantization for dissipative optical solitons," J. Opt. Soc. Am. B **27**(10), 1978–1982 (2010).
33. W. Wang, Z. Fang, T. Xian, *et al.*, "Spontaneous Synchronization and Exceptional Points in Breather Complexes," Phys. Rev. Appl. **20**(2), 024060 (2023).
34. D. Zou, Y. Song, O. Gat, *et al.*, "Synchronization of the internal dynamics of optical soliton molecules," Optica **9**(11), 1307–1313 (2022).
35. A. Blanco-Redondo, C. M. de Sterke, J. E. Sipe, *et al.*, "Pure-quartic solitons," Nat. Commun. **7**(1), 10427 (2016).
36. Y. Qi, S. Yang, J. J. Wang, *et al.*, "Recent advance of emerging low-dimensional materials for vector soliton generation in fiber lasers," Mater. Today Phys. **23**, 100622 (2022).
37. J. Peng and H. Zeng, "Build-Up of Dissipative Optical Soliton Molecules via Diverse Soliton Interactions," Laser Photonics Rev. **12**(8), 1800009 (2018).
38. Z. Q. Wang, K. Nithyanandan, A. Coillet, *et al.*, "Optical soliton molecular complexes in a passively mode-locked fibre laser," Nat. Commun. **10**(1), 830 (2019).
39. S. Yang, Z. W. Zhu, Y. Y. Qi, *et al.*, "Internal motion within pulsating pure-quartic soliton molecules in a fiber laser," Chaos, Solitons Fractals **172**, 113544 (2023).